Research Article Vol. 31, No. 2 / 16 Jan 2023 / Optics Express 2700
Optics EXPRESS

BoxCARS 2D IR spectroscopy with pulse shaping

ZIAREENA A. AL-MUALEM,[1,2] XIAOBING CHEN,[1,2] JOSEPH C. SHIRLEY,[1] CONG XU,[1] AND CARLOS R. BAIZ[1,*]

[1]Department of Chemistry, University of Texas at Austin, 105 E 24th Street, Austin, TX 78712, USA
[2]Authors contributed equally
[*]cbaiz@cm.utexas.edu

Abstract: BoxCARS and pump-probe geometries are common implementations of two-dimensional infrared (2D IR) spectroscopy. BoxCARS is background-free, generally offering greater signal-to-noise ratio, which enables measuring weak vibrational echo signals. Pulse shapers have been implemented in the pump-probe geometry to accelerate data collection and suppress scatter and other unwanted signals by precise control of the pump-pulse delay and carrier phase. Here, we introduce a 2D-IR optical setup in the BoxCARS geometry that implements a pulse shaper for rapid acquisition of background-free 2D IR spectra. We show a signal-to-noise improvement using this new fast-scan BoxCARS setup versus the pump-probe geometry within the same configuration.

1. Introduction

Two-dimensional infrared spectroscopy (2D IR) is a third-order nonlinear vibrational spectroscopy which provides bond-specific structure and sub-picosecond dynamics of molecules in the condensed phase [1–3]. Multidimensional spectra contain a wealth of structural information that is derived from the coupling between vibrational modes, producing characteristic spectral lineshapes. Dynamical information on sub-picosecond time scales, such as hydrogen-bonding lifetimes, solvent exchange rates, and conformational dynamics, are extracted from the evolution of the lineshapes as function of waiting time [1,4–7]. Two common implementations of 2D IR spectroscopy are based on the four-wave mixing "BoxCARS" and "pump-probe" geometries (Fig. 1) [2,8–10]. While the signals measured in the two geometries, are in principle, identical, there are practical tradeoffs between the two implementations: (1) in the BoxCARS configuration the signal is emitted in a background-free direction and overlapped with a reference "local oscillator" (LO) pulse for reconstruction of the signal amplitude and phase through spectral interferometry [11]. Signal-to-noise ratios (SNRs) are generally higher in the BoxCARS geometry compared to the pump-probe geometry, because the k_3 intensity can be adjusted arbitrarily, whereas in the pump-probe geometry k_3 also acts as an LO, and its intensity is therefore limited by the dynamic range of the detector. The ability to attenuate the LO is particularly beneficial when working with weak IR probes, such as thiocyanate or nitrile vibrational modes [12–14]; (2) On the other hand, the pump-probe geometry has two important advantages. First, the straightforward two-beam geometry streamlines the alignment process. Second, this geometry can be implemented using a pulse shaper which provides several advantages including fast data acquisition and scatter suppression by phase cycling [15–17]. In addition, precise control of the pulse pairs removes the need to phase spectra. However, the lack of sensitivity in the pump-probe geometry can be limiting, and indeed, chromophores with large oscillator strength are often used within this geometry. [8,18–20]

Recently, significant efforts have dedicated to improving the sensitivity of the pump-probe geometry, aiming for a background-free data collection with a pulse shaper [21–24]. Polarization schemes can be implemented in the pump-probe geometry to obviate the need to attenuate the

#471984 https://doi.org/10.1364/OE.471984
Journal © 2023 Received 28 Jul 2022; revised 31 Aug 2022; accepted 15 Sep 2022; published 11 Jan 2023

Optics EXPRESS

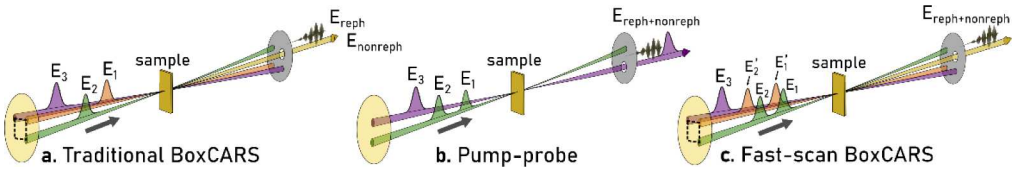

Fig. 1. Comparison of 2D IR geometries: (a) traditional BoxCARS, (b) pump-probe and (c) fast-scan BoxCARS. In the BoxCARS geometry (a, c), the four beams outline the corners of a box and the emitted signal travels in a background-free direction. In the pump-probe geometry (b), the incoming beams are collinear and the emitted signal travels in the direction of the probe beam.

probe, thereby increasing the SNR. [25,26] Xiong and Zanni adopted a polarization grating configuration in the pump-probe setup to increase the signal strength and eliminate unwanted background noise [21]. Jonas and coworkers introduced a Sagnac interferometer in partially collinear 2D electronic spectroscopy (2D ES) in order to measure a nearly background-free signal in the pump-probe geometry [22]. Fayer and coworkers enhanced the signal of monolayer/thin films by reducing the LO field without losing the signal field in a near-Brewster's angle reflection pump-probe geometry, combined with a pulse-shaping system for rapid data acquisition [23].

Inspired by the work of Ogilvie and coworkers, [24] here we report on a hybrid implementation that leverages the distinct advantages of the pump-probe and BoxCARS geometries by implementing a pulse shaper within the BoxCARS configuration. In the work of Ogilvie and coworkers, a 2D ES spectrometer with a hybrid diffractive-optic/pulse-shaping approach was introduced to measure background-free spectra in the BoxCARS geometry, however, diffractive optics have significant limitations in the IR due to the large bandwidth of the pulses compared to the center frequencies, which results in severe spatial chirp. Here we report on the design and implementation of a 2D IR setup for rapid acquisition of background-free 2D IR spectra with phase control of the pump pulses using a pulse shaper (Fig. 1(C)), which we refer to as "Fast-scan BoxCARS". This implementation combines the background-free signals from the BoxCARS geometry with the precise timing and phasing controls afforded by pulse shaping. Adopting a pulse shaper within the BoxCARS geometry allows for shot-to-shot modulation of the pump pulses, complete control of the amplitude and phase of the pump pulses, and simultaneous collection of the rephasing and nonrephasing signals. In general, our new hybrid setup provides an enhancement in SNR as compared to conventional pump-probe setups. The drawback of this setup is that the 2D IR spectra must be phased to obtain purely absorptive lineshapes.

2. Methods

2.1. *Fast-scan BoxCARS 2D IR spectrometer*

A Ti:Sapphire oscillator seeds a regeneratively amplified laser (Astrella, Coherent Inc) to output 800 nm at 7 W and a 1-kHz repetition rate. Approximately 3.5 mJ of the output is used to generate mid-IR via optical parametric amplification followed by noncollinear difference frequency generation (TOPAS Prime/N-DFG, Light Conversion), resulting in broadly tunable mid-IR pulses.

A scheme of the fast-scan BoxCARS setup is shown in Fig. 2. The mid-IR source beam is routed through a 50/50 ZnSe beam splitter (BS) to generate the "pump" (transmitted) and "probe" (reflected) beams. The pump pulse is sent through the pulse shaper (QuickShape, PhaseTech Spectroscopy), [15,27] which is based on an acousto-optic modulator (AOM), to generate a pair of time-delayed pump pulse pairs (k_1 and k_2). Electronically modulating the pump pulses allows for precise control of t_1 to eliminate timing instabilities or drift from mechanical stages used

Optics EXPRESS

in traditional BoxCARS setups. Spatial chirp from angular dispersion in the AOM is mitigated by active Bragg angle compensation in the pulse shaper. [28] A 50/50 ZnSe BS at the pulse shaper output creates a copy of the modulated output pair (k_1' and k_2'). Adding a t_1 delay between two pump pulses in each pair, the rephasing (S_R) and nonrephasing (S_{NR}) signals are simultaneously generated in same direction after the beam interactions of $S_R = -k_1' + k_2 + k_3$ and $S_{NR} = +k_1 - k_2' + k_3$, respectively. Thus, the rephasing and nonrephasing 2D IR spectra are measured together (Fig. 1).

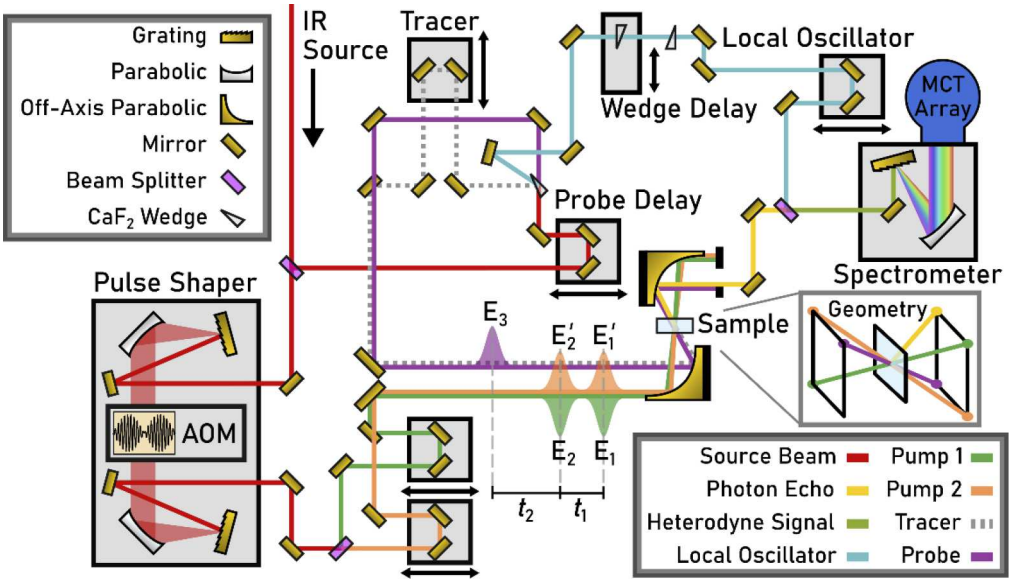

Fig. 2. Schematic view of fast-scan BoxCARS setup. The IR input is generated by a TOPAS-NDFG setup (not shown). The input pulse (red) is split by a beam splitter (BS) into two pulses. One pulse travels through the pulse shaper with an acousto-optic modulator (AOM), then a second BS, resulting in two pairs of pump pulses (E_1 and E_2, green; E_1' and E_2', orange) and each pulse pair is separated by t_1. The probe line is split into E_3 (purple), the tracer (dashed gray line), and the LO (blue) using a CaF_2 wedge. t_2 is the waiting time between the pump and probe beams. The pump and probe pulses are focused by the parabolic mirror (PM) onto the sample to generate the photon signal. The tracer tracks the direction of the emitted signal and is used as the probe in pump-probe measurements, and the LO heterodynes with the photon echo on another BS to recover the signal amplitude and phase. All beam splitters are 50/50 dielectric beam splitters on a ZnSe substrate, and the wedges are uncoated 3° CaF_2.

Optomechanical drift between the two pump arms results in phase shifts in the rephasing and nonrephasing signals. Because the signals are generated as a cross interaction between the two pump beams, any time shift, Δt, between the leading pulses, k_1 and k_1', will cause a corresponding phase shift, $\Delta\phi$, of equal magnitude and opposite signs in S_{NR} and S_R (Fig. 3). Thus, the polarization that generates the emitted electric field in this geometry becomes sensitive to these terms. The phase cycling scheme of $\phi_{12} = 0, \pi$ is used to collect signal on every shot and remove the background. The final signal maintains the phase shifts; $S \propto 2\mathrm{R}e^{i\Delta\phi} + 2\mathrm{NR}e^{-i\Delta\phi}$. However, because the coherence direction of the rephasing pathway is reversed compared to the nonrephasing pathway, $-i\Delta\phi$ will flip its sign during measurement when the negative ω_1 frequency of the rephasing pathway becomes positive. Therefore, the rephasing and nonrephasing spectra can be collected together without resulting in phase mismatch errors from drift in the pump beams. The absorptive spectra must still be phased to correct for any LO phase drift. If

Optics EXPRESS

it is desirable to collect the rephasing and nonrephasing spectra independently, one can adopt different phase cycling schemes, [15,24,29–31] including the four-frame phase cycling scheme described in Section S1.1 of the Supporting Information.

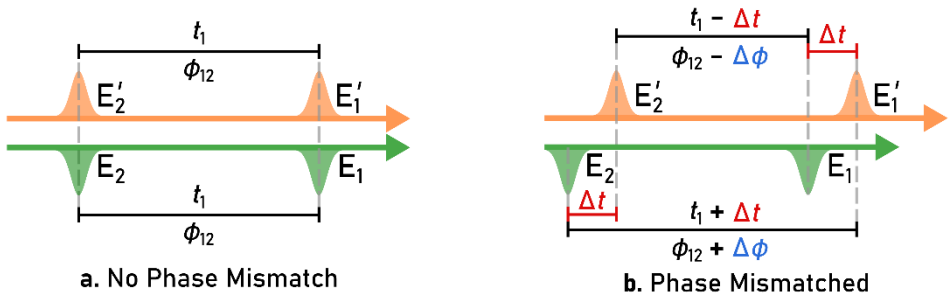

Fig. 3. Diagram demonstrating how a time shift due to optomechanical drift, Δt, between the two probe lines results in a phase shift, $\mp\Delta\phi$, in the rephasing and nonrephasing signals.

The probe pulse is split into three pulses using the front and back reflections from an uncoated 3° CaF_2 wedge: E_3 (transmitted, 95%), the tracer (reflected, 2.5%), and the LO (reflected, 2.5%). A mechanical delay stage (ANT-95 Aerotech Inc) controls the waiting time (t_2) between the pump and probe pulses. The two pump pulse pairs (E_1 and E_2; E_1' and E_2'), E_3, and the tracer are focused onto the sample area by a 10-cm off-axis parabolic mirror. The tracer beam follows the path of the generated photon echo signal from the sample and is blocked during data collection in the BoxCARS geometry. The photon echo signal and LO field interfere at a ZnSe BS to recover the amplitude and phase of the signal. The LO timing is controlled via a mechanical stage (MPS-50SL, Aerotech Inc) with a 3° CaF_2 wedge paired with a stationary CaF_2 wedge for fine control with femtosecond resolution and a manual stage for coarse timing. The heterodyned signal and LO are detected simultaneously on a 128-pixel × 128-pixel IR camera (Catalina, Teledyne Nova Sensors) [32] and the detection area is binned vertically. This hybrid BoxCARS 2D IR setup can be easily transformed to the pump-probe geometry by blocking one pump arm, E_3, and the LO, while using the tracer beam as the probe. In the signal-to-noise benchmarks below, 2D IR spectra in the BoxCARS and pump-probe geometries are collected by blocking/unblocking the appropriate beams without any additional realignment.

2.2. Sample preparation and data collection

Sodium azide (NaN_3) (99.99+%; Sigma-Aldrich) in D_2O (99.9%; Cambridge Isotope Laboratories, Inc.) samples were used to benchmark the performance of the BoxCARS implementation against the pump-probe geometry. All chemicals were used as received. The sample concentration was 50 mM and the spectra were collected at room temperature. The absorbance of the azide asymmetric stretching mode at 2043 cm^{-1} was measured to be 0.5 OD in the sample used for 2D IR. Spectra were collected in both BoxCARS and pump-probe geometries by scanning the coherence time (t_1) from 0 to 4 ps in steps of 20 fs. To reduce any unwanted pump-probe scatter and transient absorption signals, the pump was phase-cycled by shifting the relative phase between two adjacent pump pulse pairs by π, and the adjacent "0 0" and "0 π" pulse pairs are subtracted and the 2D IR signal is recovered [33,34]. The waiting times (t_2) were selected from 300 fs to 3 ps as discussed below. The rotating frame frequency was set to 1800 cm^{-1}. The excitation (ω_1) axis was generated by a numerical Fourier-transform along the t_1 delay time axis. The interference between the signal and local oscillator was measured in the frequency domain to generate the detection (ω_3) axis. Spectra were collected with all pulses in a parallel polarization geometry. Individual spectra were averaged over 50,000 laser shots and collected in five successive sets, then each spectrum was individually phased and summed

Optics EXPRESS

together to generate the final spectrum at each waiting time. A transient pump-probe spectrum was collected at a waiting time of 150 fs and used in phasing the heterodyned fast-scan BoxCARS 2D IR spectra (Figure S7). Example rephasing, nonrephasing, and absorptive spectra collected with the four-frame phase cycling scheme at a waiting time of 150 fs are included in Figure S8. Additionally, to demonstrate the capabilities of this new optical setup for fast measurement of weak vibrational probes, 2D IR spectra of 50 mM sodium thiocyanate (NaSCN) (≥98.0%; Sigma-Aldrich) in D_2O (99.9%; Cambridge Isotope Laboratories, Inc.) were collected at a waiting time of 150 fs with the same aforementioned experimental parameters. The absorbance of the nitrile stretching mode at 2067 cm^{-1} was measured to be 0.1 OD in the sample used for 2D IR.

3. Results and discussion

Example 2D IR spectra of the azide stretching mode at three waiting times collected in the fast-scan BoxCARS and pump-probe geometries are shown in Fig. 4. In brief, the spectrum shows a pair of peaks corresponding to the ground-state bleach (red feature, on the diagonal) and the excited-state absorption (blue feature, below the diagonal). In general, the BoxCARS spectra (Fig. 4) preserve the defined shape of the main peaks throughout the 3 ps measurement window (Figure S1). The minimal background in the spectra and the well-defined main peaks, even at long waiting times, highlight the quality of the spectra. It is worth noting that both the positive and negative peaks in the phased BoxCARS spectra show slight vertical elongation along the detection axis as compared to the pump-probe spectra. This can also be noted in the probe-axis projections and the diagonal slices. This peak elongation can be attributed to fifth-order signals which are more common in the BoxCARS geometry as a result of the high pulse energies [35,36].

In the BoxCARS geometry, E_3 imparts the phase onto the emitted photon echo, which is heterodyned by the LO field to determine the phase of the signal. [19,37] The heterodyned signal is phased by matching the probe-axis projection of the 2D IR spectrum to the transient pump-probe spectrum. The 2D IR spectra collected in the fast-scan BoxCARS geometry were phased by taking the real part of the product of the analytic signal and $exp(i\pi\phi)$, where ϕ is a constant phase shift in the time domain. [37] Phasing the spectra involved varying ϕ from -π to π and finding the minimum root-mean-square-difference (RMSD) between the pump-probe spectrum and the phased 2D spectrum within the phase shift range. The probe-axis projection was allowed to shift by up to 2 cm^{-1} during the calculation of RMSD minimization to account for any errors in the probe axis calibration. To correct for LO phase drifts, spectra were recorded with fewer laser shots but with more repetitions, such that each resultant spectrum can be phased individually and then averaged together at a given waiting time.

The 2D IR spectra of NaN_3 in D_2O collected in fast-scan BoxCARS geometry are compared to those collected in pump-probe geometry (Fig. 4). It is indicated that both geometries capture the same peak features in the azide stretching region. Since the spectra were normalized to the maximum absolute amplitude, it is clear that fast-scan BoxCARS spectra contain lower background noise than the pump-probe spectra at each measured waiting time. The background noise in the pump-probe spectra starts to eclipse the main peaks as indicated by the distorted contour lines of the main peaks and the relative amplitude of the noise versus main peaks. Note that the vertical stripes in 2D IR spectra indicate shot-to-shot noise. In ultrafast laser experiments, sources of noise include pulse energy fluctuations from instability in the laser output, optomechanical drift in the optical setup, and environmental factors such as air currents and thermal fluctuations. Shot-to-shot laser fluctuation from both pump and probe beams is one major noise source for 2D IR spectroscopy irrespective of the setup geometry. In addition, phase drift of the LO is another source of noise during data collection in the BoxCARS geometry.

To compare the effects of background noise in two geometries, we analyzed the pump-slice amplitudes (PSAs) for both the fast-scan BoxCARS and pump-probe 2D IR spectra (Fig. 5). PSA

Optics EXPRESS

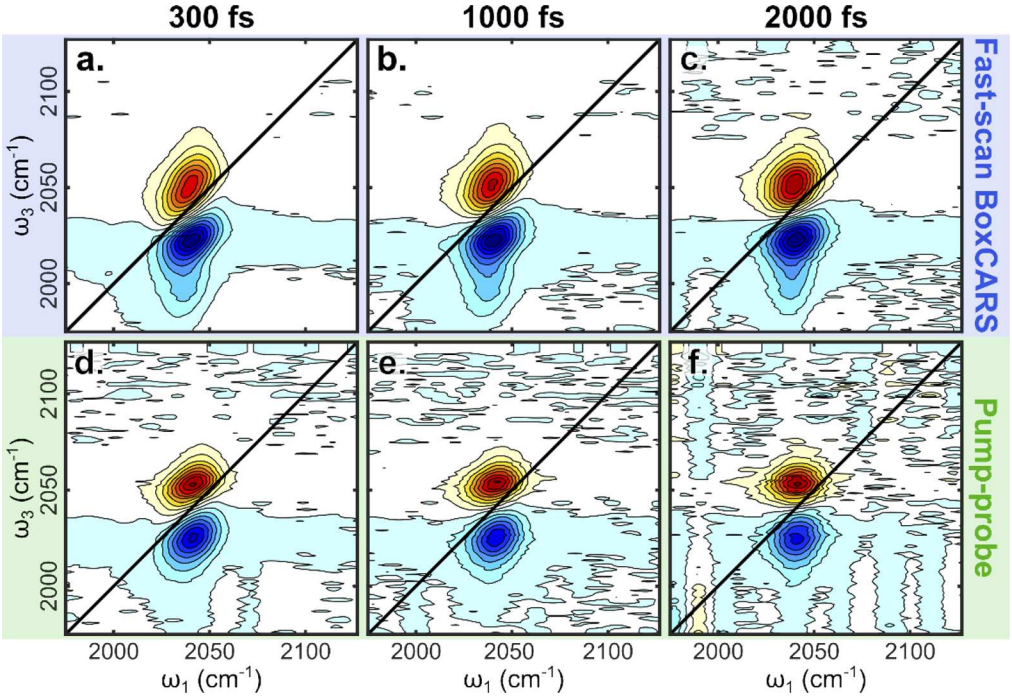

Fig. 4. Comparison of 50 mM NaN_3 in D_2O 2D IR spectra at waiting times of 300 fs (a,d), 1000 fs (b,e), and 2000 fs (c,f), collected in the fast-scan BoxCARS geometry after phasing (a-c) and the pump-probe (d-f) geometry. Each spectrum is an average of 250,000 laser shots for a total data collection time of ~5 minutes per spectrum. The spectra were normalized by the highest amplitude peak.

analysis has been described in detail previously. [38] In brief, PSA is the difference between the maximum and minimum amplitudes along ω_3 at slices along the excitation (pump) axis, which gives spectra that are comparable to the linear absorption spectra. The normalized spectra of PSAs are shown in the upper panel of Fig. 5. The PSA analysis shows that the peak widths and peak centers from the 2D IR spectra collected in the fast-scan BoxCARS geometry closely match those from the spectra collected in the pump-probe geometry. The PSAs extracted from the fast-scan BoxCARS spectra have negligible background noise so the peaks have similar baselines and lineshapes at all waiting times. PSAs at additional waiting times are included in Figure S3. However, the background noise in the pump-probe geometry becomes prominent with increasing waiting times, which distorts the background as well as the lineshapes. The improvement in the background is also investigated by the projections of the 2D IR spectra onto the detection axis (ω_3) as shown in the lower panel of Fig. 5. The positive and negative peaks in the probe-axis projection plots correspond to the positive and negative peaks in the 2D IR spectra. The projections are normalized with respect to the maximum of the positive peaks. Note that the ratio of the negative and positive peak intensities is ~-1 for the fast-scan BoxCARS geometry but is ~-0.8 for the pump-probe geometry. Due to small inaccuracies in beam alignment and the routing of the LO around the sample, the relative ratio of the negative and positive peaks is different between the two geometries. The projections from the pump-probe spectra have greater background noise as indicated by the baseline fluctuations. Similar to the PSA analysis above, the fast-scan BoxCARS geometry gives relatively baseline-free projection lines and the preserved lineshapes for the main peaks even at long waiting times. Plots of probe-axis projections at additional waiting times are included in Figure S4. The improved background noise level from

Optics EXPRESS

the fast-scan BoxCARS spectra can also be seen in the diagonal slice comparison across select waiting times in Figure S5.

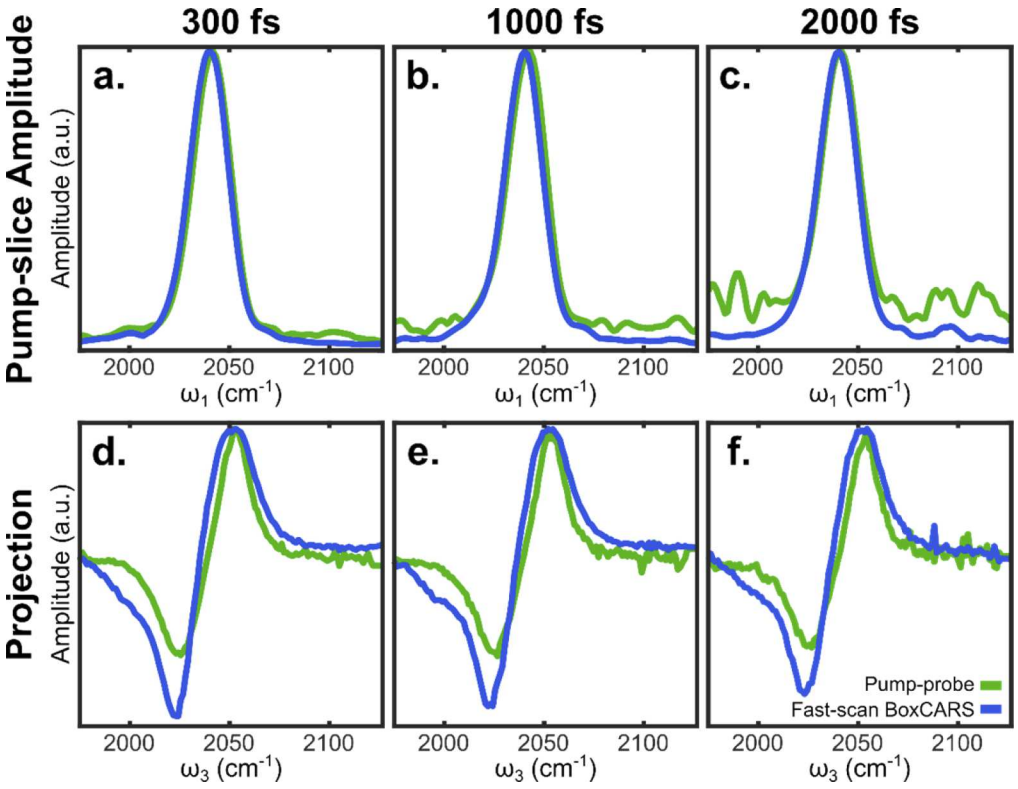

Fig. 5. Comparison of the PSA and probe-axis projections at waiting times of 300 fs (a,d), 1000 fs (b,e), and 2000 fs (c,f), for the fast-scan BoxCARS (blue) and pump-probe (green) geometries. The PSAs and probe-axis projections were calculated from the NaN_3 2D IR spectra in Figures S1-2 and were normalized to the maximum amplitude.

Signal-to-noise ratios (SNR) were calculated for each waiting time and compared between fast-scan BoxCARS and pump-probe geometries (Fig. 6(a)) in order to quantify the improvement in signal. The SNR is defined as the ratio between the maximum amplitude and the standard deviation of the baseline noise in the PSAs (Figure S6). The SNRs decrease with increasing waiting time for both geometries, but the SNR from the fast-scan BoxCARS was greater at all measured waiting times. The larger standard deviation in SNR from the fast-scan BoxCARS 2D IR PSAs at early waiting times can be attributed to the vertical elongation of the peak shapes and phase instability, as previously discussed. The ratio between the SNR of the fast-scan BoxCARS and that of pump-probe was calculated for each waiting time (Fig. 6(b)), which shows a 3× improvement in SNR for the fast-scan BoxCARS spectra versus the pump-probe geometry. This factor of 3 indicates that 9× more measurements would be necessary for the pump-probe geometry to achieve similar SNR of fast-scan BoxCARS within this current configuration.

As an additional comparison, 2D IR spectra of NaSCN in D_2O, a weak vibrational probe, are shown as an example of the fast-scan BoxCARS setup. Figure 7 shows a greater SNR for the fast-scan BoxCARS geometry over the pump-probe geometry. The PSA shows a lower noise floor in the fast-scan BoxCARS geometry (Fig. 7(c)) along with a decrease in pixel noise (Fig. 7(a)-(b)). The 2D IR lineshapes measured using the two geometries are in close agreement as there are no fifth-order contributions visible in thiocyanate spectra, unlike the azide data presented above.

Optics EXPRESS

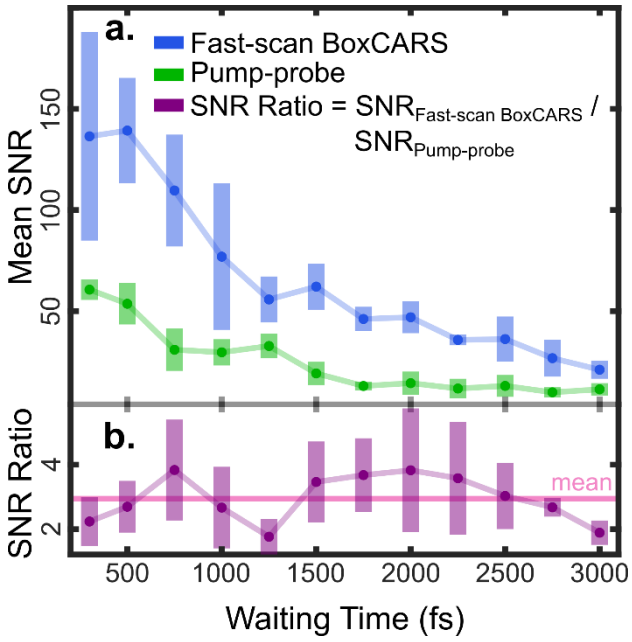

Fig. 6. SNR comparison between the two geometries. The dots represent the mean SNR from five measurements at the same waiting time with error bars (a). The solid horizontal pink line in (b) represents the mean (~3) of the SNR ratio between the fast-scan BoxCARS and pump-probe geometries across spectra measured at waiting times from 300 fs to 3000 fs.

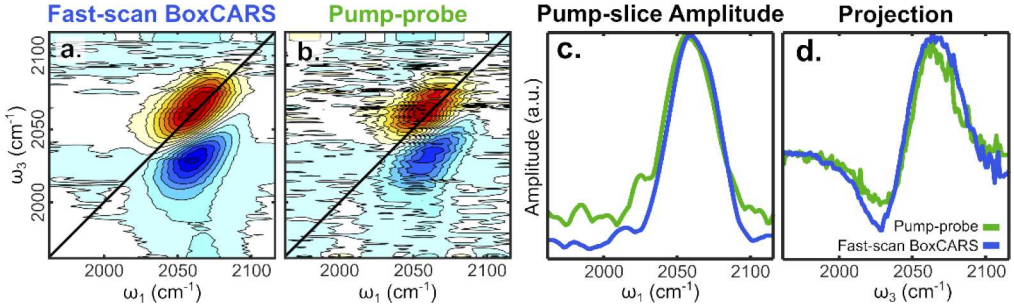

Fig. 7. Comparison of 50 mM NaSCN in D_2O 2D IR spectra at a waiting time of 150 fs collected in the fast-scan BoxCARS geometry after phasing (a) and the pump-probe geometry (b). Each spectrum is an average of 250,000 laser shots for a total data collection time of ~5 minutes per spectrum. The spectra were normalized by the highest intensity peak. Comparison of the normalized PSA (c) and probe-axis projection (d) calculated from the 2D IR spectra.

It is worth noting that data acquisition in both geometries was done with the same setup. The fast-scan BoxCARS geometry can be converted to the pump-probe geometry by using the tracer as the probe beam and blocking one of the pump beams, the E_3 beam, and the LO beam. Thus, this pump-probe setup after conversion does not have the full power for the pump and probe beams. Potentially, one can remove the beam splitter in the pulse shaper output to use the full pump power in the pump-probe geometry, thereby doubling the signal and halving the SNR improvement. Additionally, the wedge in the probe path can be replaced with another mirror as in the pump-probe geometry to obtain greater signal. Section S1.2 includes a discussion on

Optics EXPRESS

estimated signal ratios for the fast-scan BoxCARS and conventional pump-probe geometries. With this configuration, we show that without replacing optical components and by simply blocking/unblocking certain beams, we can make use of two different geometries on a single optical setup. Most significantly, the implementation of the pulse shaper in the BoxCARS geometry improves the signal-to-noise ratio in the 2D IR spectra and enables fast data acquisition of weak IR probes with phase stability and eliminated scattering artifacts. Another avenue to further increase the spectral quality is to utilize dual stripe detection. When the two stripes are phase-shifted by π, the detected heterodyned signal can be doubled by calculating the difference between the two stripes, thus eliminating the fluctuations of the LO background. Post-processing methods can also be implemented for further signal enhancement, such as denoising spectra with machine learning methods [39] and edge-pixel referencing. [40]

4. Conclusions

We demonstrate a new implementation of a BoxCARS 2D IR optical setup that affords an improvement in the quality of 2D IR spectra over the pump-probe setup by making use of a pulse shaper. It also allows for rapid acquisition of background-free 2D IR spectra with phase stability. Beyond the incorporation of a pulse shaper and beam-splitting optics, no additional or specialized optical components are necessary to implement this hybrid setup in pre-existing conventional 2D IR setups. Our work further extends the capabilities of 2D IR spectrometers in investigating weak chromophores or IR probes, such as thiocyanate and nitrile stretching probes, or dilute samples and challenging systems like transmembrane proteins.

Funding. National Institute of General Medical Sciences (R35GM133359); Welch Foundation (F-1891); Directorate for Mathematical and Physical Sciences (CHE 1847199).

Acknowledgements. Support for this research was provided by the National Institute of General Medical Sciences (R35GM133359), the Welch Foundation (F-1891), and the Directorate for Mathematical and Physical Sciences (CHE 1847199). Z.A.A. is grateful for financial support by a UT Austin Provost Graduate Excellence Fellowship.

Disclosures. The authors declare no conflicts of interest.

Data availability. Data underlying the results presented in this work are available in the URL included in Ref. [41].

Supplemental document. See Supplement 1 for supporting content.

References

1. A. L. le Sueur, R. E. Horness, and M. C. Thielges, "Applications of two-dimensional infrared spectroscopy," Analyst **140**(13), 4336–4349 (2015).
2. A. Ghosh, J. S. Ostrander, and M. T. Zanni, "Watching proteins wiggle: mapping structures with two-dimensional infrared spectroscopy," Chem. Rev. **117**(16), 10726–10759 (2017).
3. C. R. Baiz, B. Błasiak, J. Bredenbeck, M. Cho, J.-H. Choi, S. A. Corcelli, A. G. Dijkstra, C.-J. Feng, S. Garrett-Roe, N.-H. Ge, M. W. D. Hanson-Heine, J. D. Hirst, T. L. C. Jansen, K. Kwac, K. J. Kubarych, C. H. Londergan, H. Maekawa, M. Reppert, S. Saito, S. Roy, J. L. Skinner, G. Stock, J. E. Straub, M. C. Thielges, K. Tominaga, A. Tokmakoff, H. Torii, L. Wang, L. J. Webb, and M. T. Zanni, "Vibrational spectroscopic map, vibrational spectroscopy, and intermolecular interaction," Chem. Rev. **120**(15), 7152–7218 (2020).
4. M. D. Fayer, "Dynamics of liquids, molecules, and proteins measured with ultrafast 2D IR vibrational echo chemical exchange spectroscopy," Annu. Rev. Phys. Chem. **60**(1), 21–38 (2009).
5. Z. Ganim, H. S. Chung, A. W. Smith, L. P. DeFlores, K. C. Jones, and A. Tokmakoff, "Amide I two-dimensional infrared spectroscopy of proteins," Acc. Chem. Res. **41**(3), 432–441 (2008).
6. N. T. Hunt, "2D-IR spectroscopy: ultrafast insights into biomolecule structure and function," Chem. Soc. Rev. **38**(7), 1837–1848 (2009).
7. X. You, J. C. Shirley, E. Lee, and C. R. Baiz, "Short- and long-range crowding effects on water's hydrogen bond networks," Cell Rep. Phys. Sci. **2**(5), 100419 (2021).
8. L. P. DeFlores, R. A. Nicodemus, and A. Tokmakoff, "Two-dimensional Fourier transform spectroscopy in the pump-probe geometry," Opt. Lett. **32**(20), 2966–2968 (2007).
9. M. Khalil, N. Demirdöven, and A. Tokmakoff, "Obtaining absorptive line shapes in two-dimensional infrared vibrational correlation spectra," Phys. Rev. Lett. **90**(4), 047401 (2003).
10. R. Bloem, S. Garrett-Roe, H. Strzalka, P. Hamm, and P. Donaldson, "Enhancing signal detection and completely eliminating scattering using quasi-phase-cycling in 2D IR experiments," Opt. Express **18**(26), 27067–27078 (2010).

Optics EXPRESS

11. C. Dorrer, N. Belabas, J.-P. Likforman, and M. Joffre, "Spectral resolution and sampling issues in Fourier-transform spectral interferometry," J. Opt. Soc. Am. B **17**(10), 1795–1802 (2000).
12. A. C. Eckbreth, "BOXCARS: Crossed-beam phase-matched CARS generation in gases," Appl. Phys. Lett. **32**(7), 421–423 (1978).
13. X. Chen and D. G. Kuroda, "Molecular motions of acetonitrile molecules in the solvation shell of lithium ions," J. Chem. Phys. **153**(16), 164502 (2020).
14. X. Chen, Y. Cui, H. B. Gobeze, and D. G. Kuroda, "Assessing the location of ionic and molecular solutes in a molecularly heterogeneous and nonionic deep eutectic solvent," J. Phys. Chem. B **124**(23), 4762–4773 (2020).
15. S.-H. Shim and M. T. Zanni, "How to turn your pump–probe instrument into a multidimensional spectrometer: 2D IR and Vis spectroscopies via pulse shaping," Phys. Chem. Chem. Phys. **11**(5), 748–761 (2009).
16. S.-H. Shim, D. B. Strasfeld, Y. L. Ling, and M. T. Zanni, "Automated 2D IR spectroscopy using a mid-IR pulse shaper and application of this technology to the human islet amyloid polypeptide," Proc. Natl. Acad. Sci. **104**(36), 14197–14202 (2007).
17. S. C. Edington, A. Gonzalez, T. R. Middendorf, D. B. Halling, R. W. Aldrich, and C. R. Baiz, "Coordination to lanthanide ions distorts binding site conformation in calmodulin," Proc. Natl. Acad. Sci. **115**(14), 1 (2018).
18. J. C. Flanagan, M. L. Valentine, and C. R. Baiz, "Ultrafast dynamics at lipid-water interfaces," Acc. Chem. Res. **53**(9), 1860–1868 (2020).
19. P. Hamm and M. T. Zanni, *Concepts and Methods of 2D Infrared Spectroscopy*, (Cambridge University Press, 2011).
20. M. Khalil, N. Demirdöven, and A. Tokmakoff, "Coherent 2D IR spectroscopy: molecular structure and dynamics in solution," J. Phys. Chem. A **107**(27), 5258–5279 (2003).
21. W. Xiong and M. T. Zanni, "Signal enhancement and background cancellation in collinear two-dimensional spectroscopies," Opt. Lett. **33**(12), 1371–1373 (2008).
22. T. L. Courtney, S. D. Park, R. J. Hill, B. Cho, and D. M. Jonas, "Enhanced interferometric detection in two-dimensional spectroscopy with a Sagnac interferometer," Opt. Lett. **39**(3), 513–516 (2014).
23. J. Nishida, C. Yan, and M. D. Fayer, "Enhanced nonlinear spectroscopy for monolayers and thin films in near-Brewster's angle reflection pump-probe geometry," J. Chem. Phys. **146**(9), 094201 (2017).
24. F. D. Fuller, D. E. Wilcox, and J. P. Ogilvie, "Pulse shaping based two-dimensional electronic spectroscopy in a background free geometry," Opt. Express **22**(1), 1018–1027 (2014).
25. J. A. Myers, K. L. M. Lewis, P. F. Tekavec, and J. P. Ogilvie, "Two-dimensional Fourier transform electronic spectroscopy with a pulse-shaper," Opt. Express **16**(22), 17420–17428 (2008).
26. J. Réhault and J. Helbing, "Angle determination and scattering suppression in polarization-enhanced two-dimensional infrared spectroscopy in the pump-probe geometry," Opt. Express **20**(19), 21665 (2012).
27. S. H. Shim, D. B. Strasfeld, and Zanni, "Generation and characterization of phase and amplitude shaped femtosecond mid-IR pulses," Opt. Express **14**(26), 13120–13130 (2006).
28. J. M. Nite, J. D. Cyran, and A. T. Krummel, "Active Bragg angle compensation for shaping ultrafast mid-infrared pulses," Opt. Express **20**(21), 23912 (2012).
29. S. Yan and H. S. Tan, "Phase cycling schemes for two-dimensional optical spectroscopy with a pump-probe beam geometry," Chem. Phys. **360**(1-3), 110–115 (2009).
30. H. S. Tan, "Theory and phase-cycling scheme selection principles of collinear phase coherent multi-dimensional optical spectroscopy," J. Chem. Phys. **129**(12), 124501 (2008).
31. R. Duan, J. N. Mastron, Y. Song, and K. J. Kubarych, "Direct comparison of amplitude and geometric measures of spectral inhomogeneity using phase-cycled 2D-IR spectroscopy," J. Chem. Phys. **154**(17), 174202 (2021).
32. A. Ghosh, A. L. Serrano, T. A. Oudenhoven, J. S. Ostrander, E. C. Eklund, A. F. Blair, and M. T. Zanni, "Experimental implementations of 2D IR spectroscopy through a horizontal pulse shaper design and a focal plane array detector," Opt. Lett. **41**(3), 524 (2016).
33. C. R. Baiz, D. Schach, and A. Tokmakoff, "Ultrafast 2D IR microscopy," Opt. Express **22**(15), 18724–18735 (2014).
34. S. K. Karthick Kumar, A. Tamimi, and M. D. Fayer, "Comparisons of 2D IR measured spectral diffusion in rotating frames using pulse shaping and in the stationary frame using the standard method," J. Chem. Phys. **137**(18), 184201 (2012).
35. X. Zhang, R. Kumar, and D. G. Kuroda, "Acetate ion and its interesting solvation shell structure and dynamics," J. Chem. Phys. **148**(9), 094506 (2018).
36. G. Y. Jin and Y. S. Kim, "Phase-resolved heterodyne-detected transient grating enhances the capabilities of 2D IR echo spectroscopy," J. Phys. Chem. A **121**(5), 1007–1011 (2017).
37. D. M. Jonas, "Two-dimensional femtosecond spectroscopy," Annu. Rev. Phys. Chem. **54**(1), 425–463 (2003).
38. M. L. Valentine, Z. A. Al-Mualem, and C. R. Baiz, "Pump slice amplitudes: a simple and robust method for connecting two-dimensional infrared and Fourier transform infrared spectra," J. Phys. Chem. A **125**(29), 6498–6504 (2021).
39. Z. A. Al-Mualem and C. R. Baiz, "Generative Adversarial Neural Networks for Denoising Coherent Multidimensional Spectra," J. Phys. Chem. A **126**(23), 3816–3825 (2022).
40. K. C. Robben and C. M. Cheatum, "Edge-pixel referencing suppresses correlated baseline noise in heterodyned spectroscopies," J. Chem. Phys. **152**(9), 094201 (2020).
41. Raw data underlying the results of this work are available in a GitHub repository: https://github.com/baizgroup/fast-scan-boxcars-rawdata.